Structural Precursors and Electronic Structure of the Ladder Type Polymer Poly(bis(benzimidazo)benzophenanthroline) (BBB): A Combined UPS/XPS and STM Study

A. W. Munz, D. Schmeisser,* and W. Göpel

Institut für Physikalische und Theoretische Chemie, Auf der Morgenstelle 8, 72076 Tübingen, Germany

Received March 25, 1994. Revised Manuscript Received September 7, 1994[⊗]

Scanning tunneling microscopy (STM) and electron spectroscopies (XPS and UPS) are used to study the relation between the mesoscopic dynamics, the microscopic structure, and the electronic structure of polymeric bis(benzimidazo)benzophenanthroline (BBB). Semiempirical calculations are performed in order to support the geometrical and electronic structure of BBB. BBB is a conductive ladder type polymer, samples of which are prepared as thin films on SiO_2 substrates and are heat treated between 800 and 1100 K. The STM micrographs show structural features which include helical fibers coiled to strands and strands of coiled strings. These precursor structures convert via two routes that include unwinding and unravelling steps to a local condensation and ordering. The STM micrographs also reveal the dynamics of these mesoscopic precursors to microscopic structures upon annealing: For the first time in real space we follow the transition from ordered 1-dimensional domains with an aromatic corrugation to 2-dimensional arrangements with a graphitic structure. This process is considered to be a general phenomenon for pyrolytic polymers. Annealing to around 1100 K causes the formation of patches of glassy carbon within an amorphous matrix. In the electronic structure the structural transitions do not show strong variations of the relative stoichiometric values as determined form the core-level intensities but cause a semiconductor-to-metal transition as derived from the valence-band spectra. The latter may be rationalized by the formation of defects in 2-dimensional graphitic arrangements which are formed during the thermally activated reorganization of the structural elements. Such defects act as polaronic states and hence dope the polymer which ideally is semiconducting.

Introduction

In the class of organic polymers as a whole, ladder type polymers exhibit a number of remarkable properties[1] which make a systematic study of their electronic and microscopic structure[2-4] of great interest. This relates not only to their thin optical and electronic properties[5] but also to their high thermal stability which is of great technological importance.[6] The pristine ladder type polymers exhibit pronounced mechanical and thermal properties. The possibility of producing highly aligned transparent films with anisotropic optical properties—in particular the generation of spatially selective conductive patterns in such aligned transparent polymers— opens new perspectives for applications in lithography, microelectronics, optics, and molecular electronics.[3] Another approach to our current work is the understanding of the electronic contributions and their geometrical counterpart in polymers with 2-dimensional or 1-dimensional polypyrrole. There are a number of experimental features which are common to 2-dimensional polypyrrole,[7] carbon aerogels,[8] glassy carbon,[9] and BBB.[3,10,11] In particular, we refer to the similarities in the EPR[11,12] and temperature-dependent conductivity data.[13]

Pristine BBB (see Figure 1) as well as the similar BBL after polymerization are both insulating materials with an optically determined bandgap of about 2.5 eV and a conductivity in the range of 10^{-14} S cm^{-1}.[13] The conductivity of BBB films can be varied over a wide range by either Ar bombardment ($\geq 10^2$ S cm^{-1}) or temperature treatment.[14] Similar conductivities are found in BBL films with intercalated Ag^+ and Ag^0 ions/atoms.[6] Heat treatment causes an irreversible change in the conductivities: warming to 500 K causes an increase to about 10^{-9} S cm^{-1}, whereas at 800 K a

[⊗] Abstract published in *Advance ACS Abstracts,* November 1, 1994.

(1) Schlüter, A. D. *Adv. Mater.* **1991**, *3*, 282.
(2) Berry, G. C. *Polym. Eng. Sci.* **1976**, *16*, 777.
(3) Coter, F.; Beliash, I.; Davidov, D.; Dalton, L. A.; Ehrenfreund, E.; McLean, M. R.; Nalwa, H. S. *Synth. Met.* **1989**, *29*, E471. Belaish, I.; Davidov, D.; Selig, H.; McLean, M. R.; Dalton, L. *Adv. Mater.* **1989**, *11*, 387.
(4) Van Deusen, R. L.; Goins, O. K.; Sicnee, A. T. *J. Polym. Sci. A-1* **1968**, 1777.
(5) Dalton, L. R.; Thompson, J.; Nalwa, H. J. *Polymer* **1987**, *28*, 543.
(6) Jenekhe, S. A. *Polym. Mater. Sci. Eng.* **1989**, *60*, 419.
(7) Bartl, A.; Dunsch, L.; Naarmann, H.; Schmeisser, D.; Göpel, W. *Synth. Met.* **1993**, *61*, 167.
(8) Fung, A. W. P.; Wang, Z. H.; Lu, K.; Dresselhaus, M. S.; Pekala, P. W. *J. Mater. Res.* **1993**, *8*, 1875.
(9) Heiduschka, P.; Munz, A. W.; Göpel, W. *Electrochim. Acta.* **1994**, *39*, 2207.
(10) Bätz, P.; Schmeisser, D.; Göpel, W.; Belaish, I.; Davidov, D. Conf. Proc. ICSM'90, Tübingen, *Synth. Met.* **1991**, *42*, 1449.
(11) Davidov, D.; Belaish, I.; Rettori, C.; McLean, M. R.; Dalton, L. R. *Polym. Adv. Techn.* **1990**, *1*, 181.
(12) Belaish, I.; Rettori, C.; Davidov, D.; McLean, M. R.; Dalton, L. R.; Nalwa, H. *Mater. Res. Soc. Symp. Proc.* **1989**, *134*, 689.
(13) Kim, O.-K. *Mol. Cryst. Liq. Cryst.* **1984**, *105*, 161.
(14) Jennings, B. R.; Ridler, P. J. *Polymer* **1987**, *28*, 741.

0897-4756/94/2806-2288$04.50/0

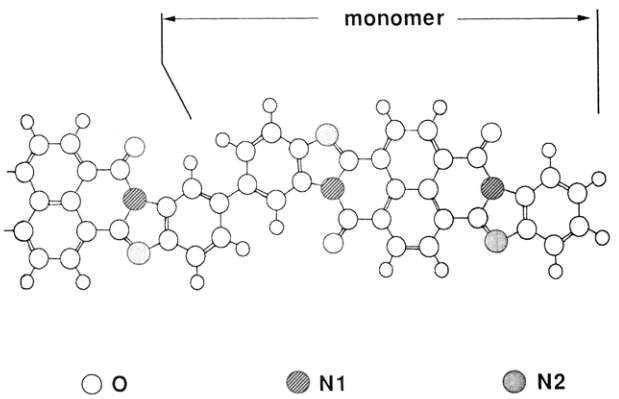

Figure 1. Schematic representation of the chemical structure of the monomer unit of BBB. The displayed arrangement is obtained after a force field and semiempirical MNDO optimization.

further increase to 10^{-6} S cm^{-1} is observed (measured at room temperature).[11,13] A further increase in conductivity of several orders of magnitude is obtained upon warming the films to 950 K. The conductivity reaches values around 50 S cm^{-1} at still higher temperatures. In this state, the conductivity shows a normal to parallel anisotropy of around 1/1000 and is almost independent of the heat treatment. This thermally induced conductivity change can also be obtained by laser irradiation, which has the advantage of writing conductive patterns in a transparent insulating polymer.[3] The conductivity increase upon heat treatment is also reflected in the corresponding EPR data. The spin densities increase to a value of around 10^{22} spins/mol for films heated to 980 K followed by a sharp decrease to densities below 10^{20} spins/mol upon heating above 980 K.[11,12]

The ladder type polymers in general show a rather high degree of ordering as deduced from the appearance of diffraction spots in X-ray analyses. For BBB films, diffraction spots indicate mean distances between conductive structures to be 8.2 Å, with a next-neighbor distance of 3.2 Å within the polymeric features.[2] These data suggest the structure of this ladder type polymer to be close to that of the layered form of graphite. BBB films exhibit pronounced changes in their phenomenological properties upon annealing, which resemble to the general features of pyrolytical polymers.[15–19]

Previously, we investigated the chemical and electronic properties of heat-treated BBB films using XPS, TDS, HREELS, and UPS spectroscopies.[10] Again, the results allow two different phases of BBB films to be distinguished. The XPS data underline the thermal stability of such films as the C/N ratio in the high-temperature metallic state is independent of the annealing temperature. There is a weak but pronounced change occurring around 950 K which can be understood as separating the two phases with similar overall stoichiometries but with distinct differences in the electronic properties. In the TDS data, loss of nitrogen is observed, but no desorption of the monomeric molecular unit. This behavior indicates that the annealing does not cause a desorption of fragments and of incompletely polymerized species, but rather leads to a reorganization on a molecular scale.

The discussion of conductivity in organic polymers lacks a detailed knowledge of their geometric structure, in both microscopic and mesoscopic dimensions. Recently, we have been able to elucidate the microscopic structure of 2-dimensional polypyrrole films by the use of electron spectroscopies and semiempirical model calculations.[7] For the BBB films we combined these techniques with the real space structural informations obtained by STM.

There are a number of STM studies on organic materials which intend to use the molecular resolution available with this technique as an analytical tool in probing these materials.[20–22] A number of studies demonstrate that for some organic materials STM can be used with atomic resolution. Among these are several impressive studies on charge-transfer salts which demonstrate atomic resolution in determining the position of individual atoms within the surface unit cell[23–25] and their electronic properties.[26] A further class of materials are thin films prepared by sublimation or by Langmuir–Blodgett techniques on substrates of layered compounds (WSe_2, MoS_2, HOPG, graphite, etc.).[22,27,28] The mechanisms causing the contrast of the STM images and in particular that of the tunneling current are not understood in detail yet.[28,29] However, to obtain good resolution and reliable STM micrographs, the samples must have certain properties which include smoothness (on a microscopic scale), immobilized structural features, and high conductivity. These conditions cannot easily be reached, in particular, for polymeric samples. As a consequence, the number of investigated polymeric systems is limited to a few studies of conducting polymers,[30,31] thin polymeric films on a conducting substrate,[32] and metallized polymers.[33] However, none of these studies gives information on the mesoscopic dynamics of the polymer strands, but they do give some indication of the existence of several helical features in an unstructured matrix.[34]

The aim of the present study is to follow in real space the changes in BBB films around the structural transi-

(15) Burger, A.; Fitzer, E.; Heim, M.; Terwiesch, B. *Carbon* **1975**, *13*, 149.
(16) Inagaki, M.; Harada, S.; Sato, T.; Nakajima, T.; Horino, Y.; Morita, K. *Carbon* **1989**, *27*, 253.
(17) Hishiyama, Y.; Yasuda, S.; Yoshida, A.; Inagaki, M. *J. Mater. Sci.* **1988**, *23*, 3272.
(18) Hishiyama, Y.; Yoshida, A.; Kaburagi, Y.; Inagaki, M. *Carbon* **1992**, *30*, 333.
(19) Hatori, H.; Yamada, Y.; Shiraishi, M. *Carbon* **1992**, *30*, 763.
(20) Fuchs, H. Atomic Force and Scanning Tunneling Microscopies of Organic Surfaces. Opening Lecture, XXI European Congress of Molecular Spectroscopy (EUCMOS XXI), *J. Mol. Struct.*, in press.
(21) Rabe, J. P. *Ultramicroscopy* **1992**, *42–44*, 41.
(22) Frommer, J. *Angew. Chem.* **1992**, *104*, 1325.
(23) Sleator, T.; Tycko, R. *Phys. Rev. Lett.* **1987**, *60*, 1418.
(24) Bar, G.; Magonov, S. N.; Cantow, H.-J.; Gmeiner, J.; Schwoerer, M. *Ultramicroscopy* **1992**, *42–44*, 644.
(25) Rabe, J. P.; Buchholz, S. In *Conjugated Polymeric Materials: Opportunities in Electronics, Optoelectronics, and Molecular Electronics*; Bredas, J. L., Chance, R. R., Eds.; NATO-ARW Series E; Kluwer: Dordrecht, 1990; p 483.
(26) Schmeisser, D.; Naarmann, H.; Göpel, W. *Synth. Met.* **1993**, *59*, 211.
(27) Foster, J. S.; Frommer, J. E. *Nature* **1988**, *333*, 542.
(28) Fuchs, H.; Akari, S.; Dransfeld, K. *Z. Phys. B* **1990**, *80*, 389.
(29) Ludwig, C.; Gompf, B.; Glatz, W.; Petersen, J.; Eisenmenger, W.; Möbus, M.; Zimmermann, U.; Karl, N. *Z. Phys. B* **1992**, *86*, 397.
(30) Jeon, D.; Kim, J.; Gallaghar, M. C.; Willis, R. F.; Kim, Y.-T.; *J. Vac. Sci. Technol. B9* **1991**, *2*, 1154.
(31) Naoi, K.; Oura, Y.; Okamoto, Y.; Oyama, N. Conf. Electrochem. Soc., Interface, Springer 1993, Abstract No. 1945, 2654.
(32) Hawley, M. E.; Benicewicz, B. C. *J. Vac. Sci. Technol.* **1991**, *B9(2)*, 1141.
(33) Piner, R.; Reifenberger, R.; Martin, D. C.; Thomas, E. L.; Apkarian, R. P. *J. Polym. Sci. (Polym. Lett.)* **1990**, *28*, 299.
(34) Yang, R.; Evans, D. F.; Christensen, L.; Hendricksen, W. A. *J. Phys. Chem.* **1990**, *94*, 6117.

tion which occur between 900 and 1000 K in real space utilizing scanning tunneling microscopy (STM). For the first time to our knowledge it is demonstrated that a direct observation of macroscopic changes in bulk polymers by STM is possible for mesoscopic structures. The observed patterns start with mesoscopic structures ranging between 100 and up to 500 nm. The STM images also reveal the molecular corrugation of BBB within the films. The observed patterns describe the changes below and beyond the structural transition caused by thermal annealing. In addition, we studied the effect of temperature on the electronic structure of BBB films by photoelectron spectroscopies. The structural changes as observed in the STM patterns, as well as the variations occurring in the electronic structure as followed by UPS, are supported by semiempirical MNDO calculations. They also contribute to understand and to elucidate the origin of the strong conductivity increase as a function of the annealing temperature.

Experimental Section

Synthesis of the BBB Films. Monomeric BBB (see Figure 1) was dissolved in methanesulfuric acid. With a pipet some milliliters of the monomeric solution were deposited onto a SiO_2-covered Si(001) wafer as a smooth substrate. Next, the solution coated substrate was dipped into water to start the polymerization reaction. All of these preparation steps of the BBB films were performed in a nitrogen atmosphere. The resulting BBB films (with a thickness around 10 μm) appeared as a solid phase and showed a dark violet color. Afterward, the films were transported to the UHV system without exposure to air. This delicate procedure allows the use of surface-sensitive techniques for the determination of bulk electronic structure without any surface contamination of the samples.[35] The polymerization procedure was followed by a heat treatment of the BBB films in a vacuum vessel for several hours at temperatures of 900, 980, and 1120 K. Thereby, we obtained heat-treated BBB samples below and above the characteristic temperature of 950 K at which the structural transition is expected from the conductivity data.[11,12]

STM Measurements. The STM experiments were performed with a commercial microscope described elsewhere.[36] All measurements were done in air at room temperature and the patterns are taken in the constant-current mode. Patterns with best resolution could be achieved by using electrochemically etched tips of tungsten wires (0.25-mm diameter). The sample bias voltages applied have been varied over a wide range, the value of which depends sensitively on the particular scan size and the particular heat treatment of the BBB films. To give some examples, images of BBB films annealed at 980 K and BBB films annealed at 1150 K could be obtained only with an optimum resolution by using tip voltages around 0.0 V a current of 0.4 nA. On the other hand, the large scan size used for the topological micrographs covered areas between about 60 nm up to 510 nm and were recorded using tip voltages of +0.6 V (current 0.4−1.0 nA). Imaging the molecular corrugation of BBB films annealed to 900 K was accomplished by using tip voltages of about −0.35 and a 0.5−0.7 nA tunneling current. Recordings of the surface by large scan sizes were taken at values between −1.0 and +1.5 V (current 0.4−0.9 nA). In all the figures displayed in this work the scan parameter (scan size, tip current, and tip tunnel voltage) are given in parentheses in the figure captions.

We like to mention that we have attributed particular care to avoid the interpretation of artifacts in the STM micrographs caused by tip effects. Artifacts may be originated by electronic noise, resonances in the feedback loop, tips contaminated by polymer fragments, or others. On polymeric samples with rough and nonordered surfaces we may also expect artificial structures caused by the scanning tip. To separate such artifacts from the real surface structure, we applied several several commonly used procedures. Real structures are expected to show identical features with high reproducibility. The micrographs shown here are found to occur in a similar shape on different samples. The patterns show no significant changes from one scan to the next scan. In particular, they are found to be independent of the scan parameters used, such as scan frequency, size, and direction. Furthermore, the micrographs remained qualitatively invariant to the exchange of the tip. Thereby, the contribution of artifacts to the observed surface structure is minimized by such tests during the measurements.

XPS/UPS Measurements. The electron spectroscopies are done in a UHV system operated at a base pressure better than 10^{-10} mbar using a hemispherical energy analyzer. XPS spectra are excited by Mg Kα radiation and valence band spectra by a He resonance lamp.[37] The elemental composition of the films was followed by XPS, the valence band structure was studied by UPS, and the vibronic and electronic range near the HOMO−LUMO transitions were determined by HREELS. The spectra are taken at room temperature after annealing the films to a defined temperature for 5 min. The annealing procedure causes irreversible changes within the films, the nature of which depends on the annealing temperature. At all temperatures any intensity of Si2p substrate emission was not detectable in the XPS spectra. This means that even after the annealing process the thickness of the polymer film is larger than the information depth of the Si2p photoelectrons.

Results

STM Micrographs. For the STM studies we used BBB films prepared on the natural oxide of polished Si wafers. These films had a thickness about 10 μm and appeared optically smooth. For BBB films annealed to 900 K we are able to identify various mesoscopic structures which will now be described. We like to mention that the features in these patterns are observed in different regions of the wafer in similar shape and dimensions. These patterns therefore are considered to represent the real structure and tip effects certainly can be excluded. This chapter is organized as a description of the results in a sequence which is maintained in the subsequent interpretation section. The structural rearrangements in the bulk polymer caused by the annealing procedure near the structural transition around 980 K starts with a macroscopic 1-dimensional polymeric precursor structure (Figure 2). It subsequently undergoes structural variations and converts along two possible routes (Figures 3 and 4) toward the microscopic graphitic structure which finally appears above the structural transition (Figures 6 and 8).

Structures of the Low-temperature Phase (900 K). The structures displayed in the following micrographs certainly represent the bulk properties of the BBB films because of their large thickness. To describe these structures in detail, we show in Figure 2 STM micrographs with a scan size of 510 nm on a BBB film annealed to about 900 K. We identify polymer cords which are aligned almost in parallel with each other (Figure 2A). The average length of the cords is of the order of several hundred nanometers, and an average

(35) Bätz, P.; Schmeisser, D.; Göpel, W. *Solid State Commun.* **1990**, *74*, 461; *Phys. Rev. B* **1991**, *43*, 9178.
(36) Besocke, K. *Surf. Sci.* **1987**, *181*, 145.
(37) Rager, A.; Gompf, B.; Dürselen, L.; Mockert, H.; Schmeisser, D.; Göpel, W. *J. Mol. Electron.* **1989**, *5*, 227.

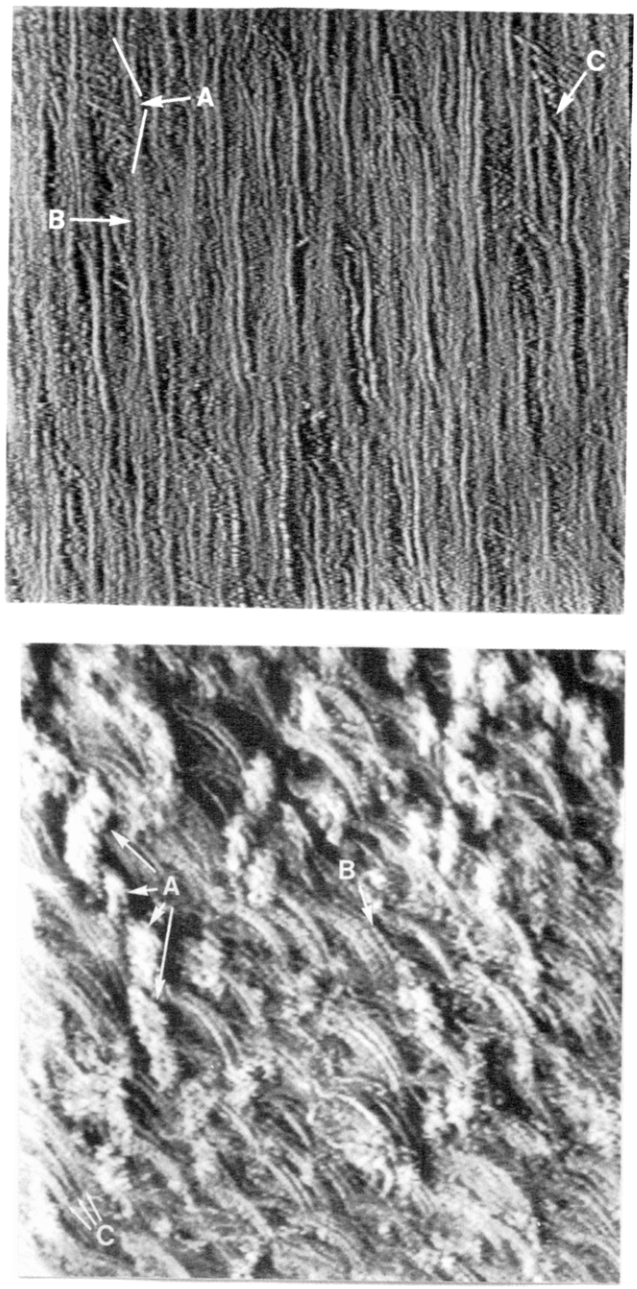

Figure 2. STM micrographs of BBB films on a Si(001) wafer after annealing to 900 K. (A, top) The 1-dimensional polymer cords have an average width of 7.3 nm and a length of several tens of nanometers. They are aligned almost in parallel. The A indicates an unravelling cord along the bars, B the segmentation of a wound polymer cord, and C points to a cross connection between cords (510 nm, +0.95 V, 0.3 nA). (B, bottom) The micrograph shows a rudimentary cord consisting of four segments (four arrows next to A). B points to a segmented cord of smaller dimensions, and C points to three wound double cords (510 nm, +1.39 V, 0.7 nA).

cord width of 7.0 nm was evaluated. The uniform appearance of the cords at some sites is disturbed by additional features. In Figure 2 these are labeled A–C. Along the bars A a network of smaller polymer cords occur. B points to a cord showing a segmentation. The arrow C indicates one of the few cross-linkings.

At a different region of the sample we find an image (observed with the same scan size) as displayed in Figure 2B. Here, we observe structures very similar to the cords also, but with a light curvature. We also notice on a larger scale rudimentary segments of larger cords A with an average diameter of several tenths of a nanometer. There are several of these rudimentary, unraveled segments of large cords randomly distributed all over the image. In this respect the region marked A shows the development of an unravelling process which leads to a matrix of less-aligned cords. The latter are also twisted (B) and cause an undulating topology. Here, the average cord width is about 5.7 nm (see Figure 5B). This micrograph clearly shows the segmentation of the smaller cords generating the matrix (B). Furthermore, there are three helical double cords which are indicated by C.

The unwinding processes shown in Figure 2 are expected for polymers, we feel that the STM micrographs in Figures 3 and 4 can be analyzed in such a way that there are two possible routes (A, B) toward a structural transformation. Both routes start with the macroscopic cords, which via different unravelling processes then lead to a planar arrangement of aromatic units. The first possible mechanism (route A) proceeds via an unravelling and cross-connecting of helical cords (Figure 3), whereas in the second mechanism (route B) the cords unravel to form structures which resemble scales (Figure 4).

Starting with the first of the routes in Figure 3A we find a zigzag pattern of these polymer cords running parallel to the surface plane. The two main orientations within the pattern are marked (*a*) and (*b*) and include an angle of about 60°. In contrast to (*a*), direction (*b*) is nearly uniform. Angles of 120° also appear but are rare (A).

In Figure 3B, the pattern is built up by unraveled cords and the parallel arranged subunit cords to create ribbons. The recorded framework shows the main directions *a*–*c*. It is very similar to the one described in Figure 3C with regard to the triagonally elements. The main direction of cords within the matrix is *a*. The two other directions *b* and *c* indicate the direction of the triangle sides. The sides are not straight but weakly bent. The first arrow on the left-hand side of the image indicates the direction of a neighboring cord. The following arrows mark seven individual turns of the cord. Each turn causes the cord to become broadened and the resulting structures consist of smaller cords which are arranged in parallel.

Figure 3C shows a complicated framework of polymer cords of different widths. At first glance a triangular pattern is observed with angles close to 30°, 60°, and 120°. However, the main elements of that arrangement are not these triangles but ribbons consisting of parallel cords running randomly in a helical manner. Four arrows on the left (and right) side indicate the way in which such a ribbon turns three times through an angle of 60° and takes on a flat compressed helical shape. The angle of fold (bars) is 120°. The main structural elements in Figure 3D are rolls which propagate in a direction diagonal to the scanning direction (parallel to the upper edge of the image) and have a length of several tenths of a nanometer (A). The rolls are segmented in scales of ellipsoidal shape (A) and are built up by sequences of triagonally shaped structural elements, each lying behind the other like fallen dominos (B).

The structural features of the second unravelling route are described in Figure 4. In Figure 4A we show

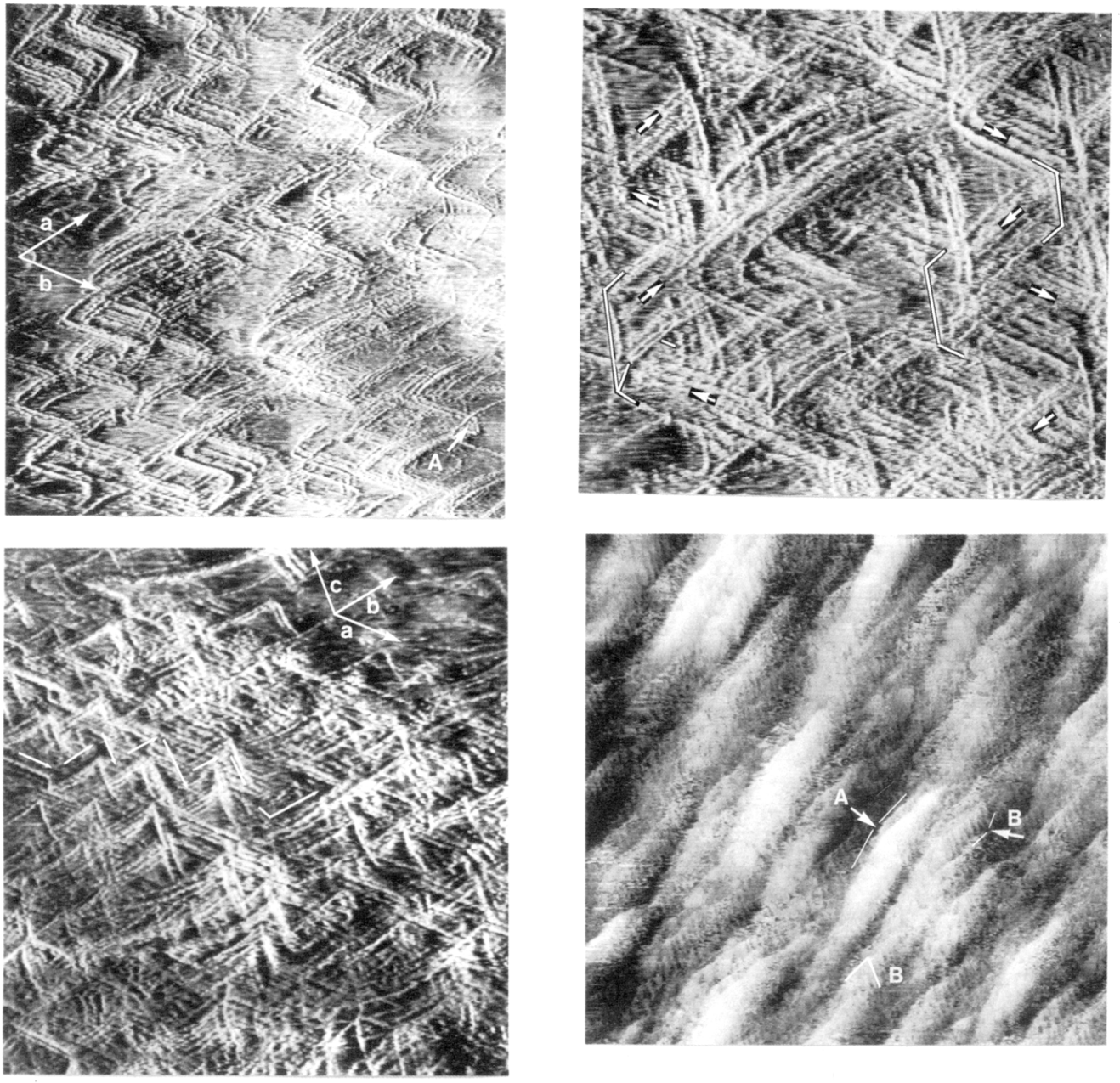

Figure 3. Unravelling of large polymer cords via route A (see text and Figure 13) obtained by annealing BBB films to 900 K. (A, top left) Zigzag pattern of polymer cords running parallel to the surface plane. The two main orientations within the pattern are marked (a) and (b) and include an angle of about 60°. Angles of 120° (A) are rare (510 nm, +1.24 V, 0.9 nA). (B, bottom left) The pattern consists of large cords which are unravelled and create smaller polymer ribbons. The arrows on the left-hand side follow the unravelling of a large cord (510 nm, +0.65, 0.7 nA). (C, top right) Framework of polymer cords consisting of triagonal structure elements. The pattern is built up by helically shaped polymer ribbons. The series of arrows on the left- and right-hand sides show the propagation of two multiple folded ribbons. The folding angle is close to 120° and is indicated by the black bars (256 nm, +1.08 V, 0.7 nA). (D, bottom right) Undulated surface consisting of rolls (A) running in the diagonal direction. The rolls are built up by triangles standing behind each other (B) (256 nm, −0.54 V, 0.5 nA).

a region of a BBB film annealed to 900 K which shows a random distribution of scale-like structures (A). The diameter of the scales varies between 50 and 100 nm and their shape is nearly spherical. Within each scale there appear ribbonlike structures consisting of parallel polymer cords.

Figure 4B shows an undulating surface with a triangular fish-scale structure. Here the scales are built up by polymer cords which have an almost uniform orientation (*a*). We notice that most of the parallel aligned cords extend over more than a single scale (follow the directions of *a*). The average cord width within the scales is reduced to 4.1 nm (Figure 5c).

In Figure 4C the image again reveals an undulating surface. Its shape can be described as a synthesis of the two other figures (Figures 4A and 3B). Within that undulating surface, both spherical and triangular scales can be observed which contribute to the main orientation (*a*). We further notice that the fine structure within the scales consists of parallel polymer cords propagating (roughly) in the direction of *b*.

Structures of the High-Temperature Phase BBB 980 K. In the high-temperature phase (annealing to 980 K) the variety of different structural elements becomes reduced, the polymer structures demonstrated in Figures 3B and 4C disappear upon annealing, and there

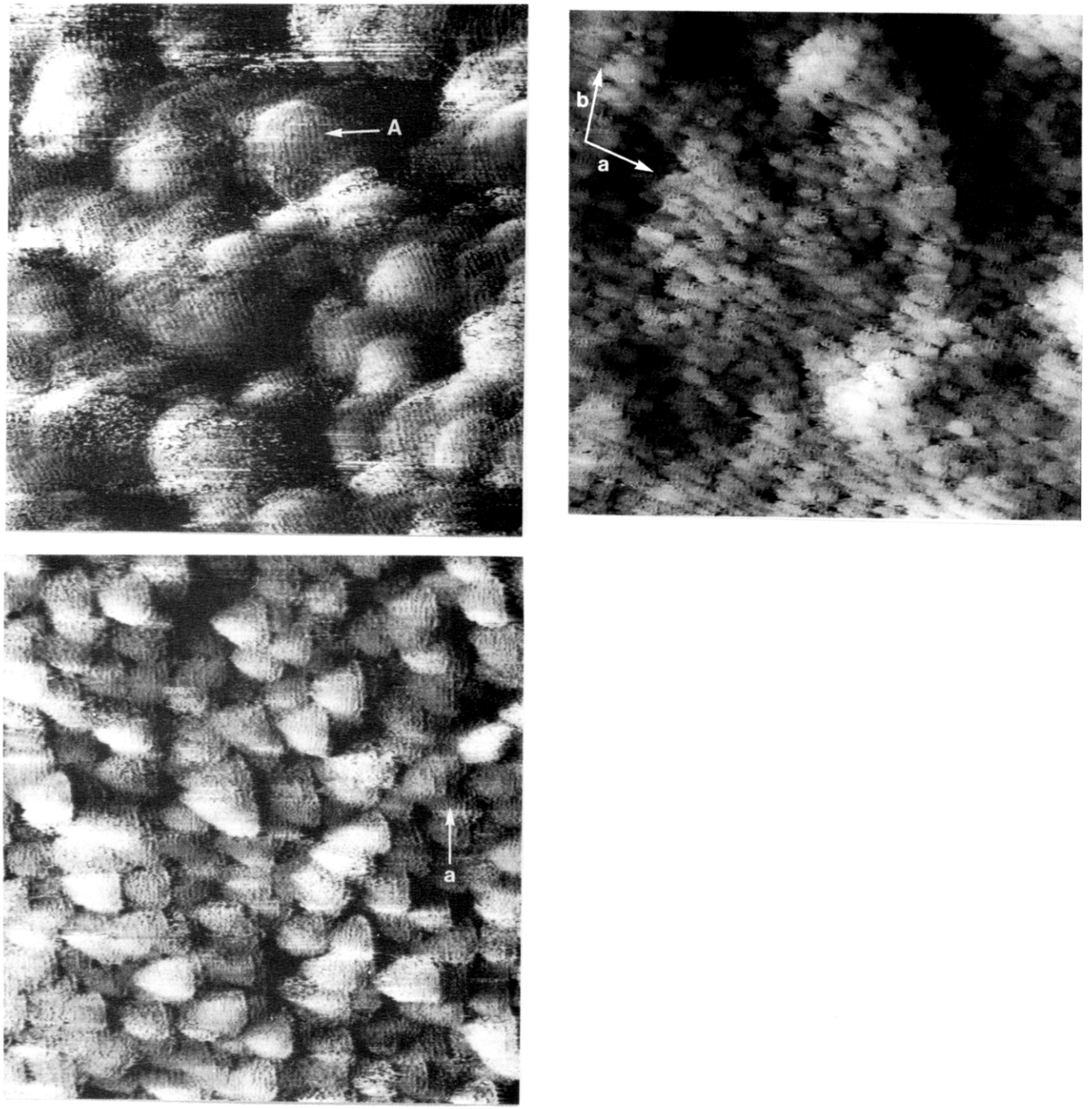

Figure 4. Second observed route B of unravelling large polymer cords. The sequence is built up by patterns observed on BBB films annealed to 900 K. (A, top) The surface consists of scales (A) showing a nearly spherical shape. The fish-scale-like structures were built up by parallel polymer cords with an average width of about 3.7 nm (256 nm, −0.34 V, 0.8 nA). (B, middle) The scales are built up by parallel polymer cords which are slightly curved and have an average width of 4.2 nm. The pattern reveals the condensation of a triagonally fish-scale structure (510 nm, 1.0 V, 0.6 nA). (C, bottom) The scales appear at different sites and appear either with a spherical or triagonal shape. The scales are aligned to form ordered elements which define the direction (a). They are built up by polymer cords running in the direction of b. The image can be described as a synthesis of 4A and 4B (510 nm, −0.72 V, 0.5 nA).

are no longer polymer cords as observed in Figures 2. In Figure 6A we notice a relationship with the structure of Figure 4C, but the surface shows no spherical or triagonal scales. The structure is dominated by flakes which show only a weak orientation. There are further similarities which become evident by a comparison of Figure 6B and Figure 3D. In Figure 6B ellipsoidic shaped scales are evident which are built up into rolls aligned to run along the direction a. Some segments or scales (e.g. A) show a fine structure which is along the direction of b. Triangular-shaped structural elements do not exist.

High-Resolution Measurements. For BBB films annealed to 900 K and BBB films annealed to 980 K we have been able to perform high-resolution measurements at several sites of the samples. Figure 7 shows data for the low-temperature phase with the best achievable resolution. The image is recorded from the middle part of Figure 4C and reveals a complex surface of more or less well ordered structural elements: these elements show an orientation in the direction of a. A frequently occurring structural element on the surface is indicated H, which shows a scale with a diameter of about 3.5 nm. We would like to focus on a further detail

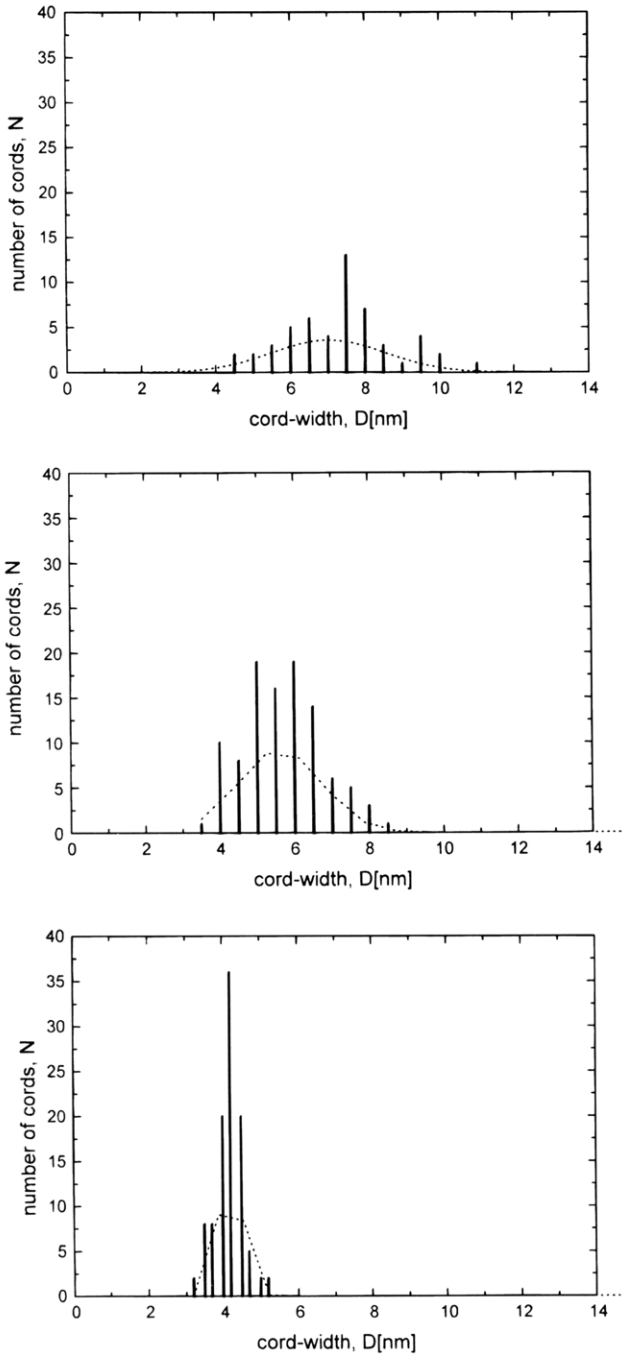

Figure 5. Histograms of the cord-width distribution. (A, top) The distribution of the precursor-like structure obtained from Figure 2A. The curve is continuous between 4.0 and 11.0 nm. The average cord width is about 7.3 nm. (B, middle) Taken from Figure 2B, showing a distribution of smaller cord widths ranging between 3.5 and 9.0 nm. The average width is reduced to about 5.7 nm. (C, bottom) Data taken from Figure 4B. The cord widths range between 3.0 and 5.0 nm and show an average width of about 4.2 nm.

indicated with A. The arrows A are pointing to some parallel structure. The distance between the arrows corresponds to the corrugation width and amounts of 0.47 nm (±0.02 nm). This distance is significant and rather uniform within this detailed micrograph.

As a consequence of the smaller dimensions sampled in these micrographs, the tip-induced artifacts may contribute and cause artificial structures. However, double- or multiple-tip images as well as resonances in the feedback loop appear usually along the direction of

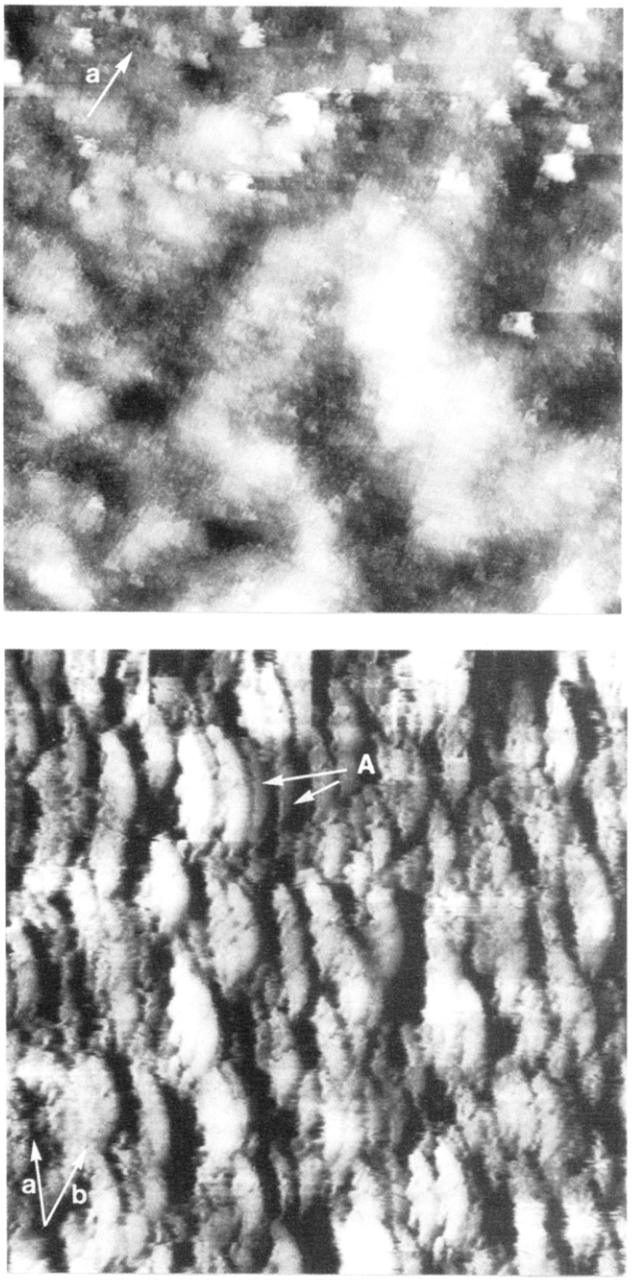

Figure 6. STM micrographs of a BBB film on a Si wafer annealed to 980 K. (A, top) Characteristic structure of BBB films annealed to 980 K. The structure is built up by flakes which are rather similar in size. The flakes show a weak orientation along (*a*). 1-Dimensional polymeric structures no longer occur and have been transferred into 2-dimensional planar features (510 nm, +0.62 V, 1.0 nA). (B, bottom) Second structural element. The surface shows rolls consisting of segments A in a uniform orientation (*a*). They have a weak, fine structure oriented along *b* (510 nm, +0.60 V, 0.9 nA).

the scan which is not the case in the images of Figure 7. We also find the width of the corrugation to be independent of the scan size, which is a further indication that the imaged structures do correspond to the real space topology. The image of the high-temperature phase of Figure 8 is recorded from the middle part of Figure 6A. At first glance the structure seems to be very similar to that recorded on the low-temperature phase (Figure 7). The surface also consist of scales (H) or flakes with diameters of 3−5 nm showing a corrugation with the main direction of *a*. The corrugation width (distance between the (A) arrows) is about 0.24 nm (±0.02 nm).

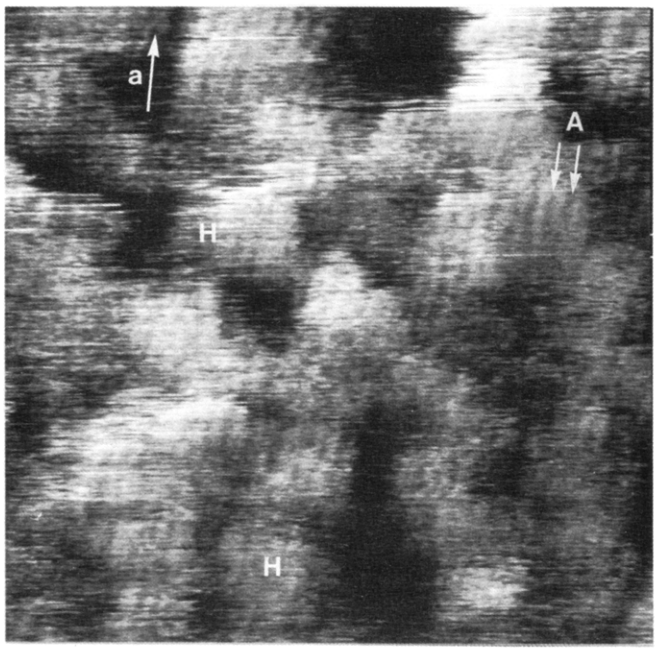

Figure 7. High-resolution image of the low-temperature phase BBB annealed to 900 K. The micrograph reveals the molecular corrugation of the polymer with an orientation in the direction of *a*. The A arrows indicate the corrugation width within the polymer structure which is about 0.5 nm. (16.0 nm, −0.35 V, 0.3 nA).

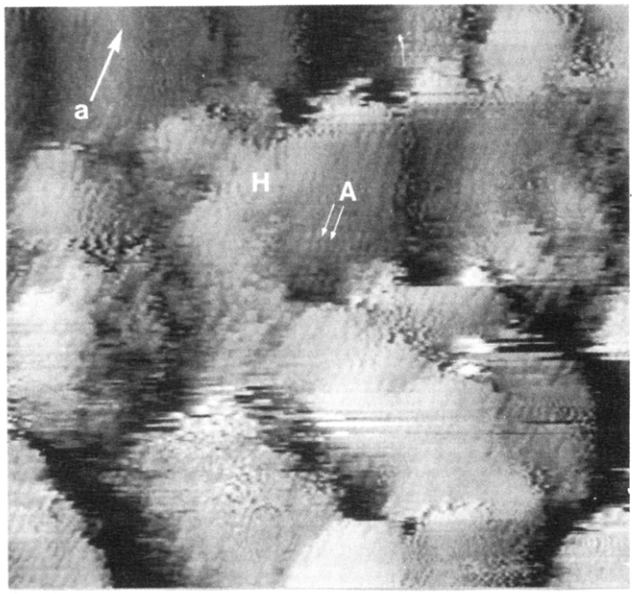

Figure 8. High-resolution image of the high-temperature phase BBB annealed to 980 K. The image shows the raw data, the surface shows corrugated flakes (H) with diameters of about 3 nm. *a* indicates the main direction of the corrugation. The corrugation width (distance between the A arrows) on a scale (H) is about 0.23 nm (16.0 nm, 0.0 V, 0.4 nA).

XPS/UPS Measurements. In the context of our comparative STM-XPS/UPS studies we would now like to focus on the changes which appear in the XPS and UPS spectra induced by annealing and in particular to those which occur around the structural transition at temperatures near 950 K. In Figure 9A the N1s spectrum of a BBB-film annealed to 980 K is displayed which shows two clearly resolved components with binding energies at 398.7 and 400.8 eV. This remarkable emission pattern is observed at all temperatures except immediately after preparation of the films at

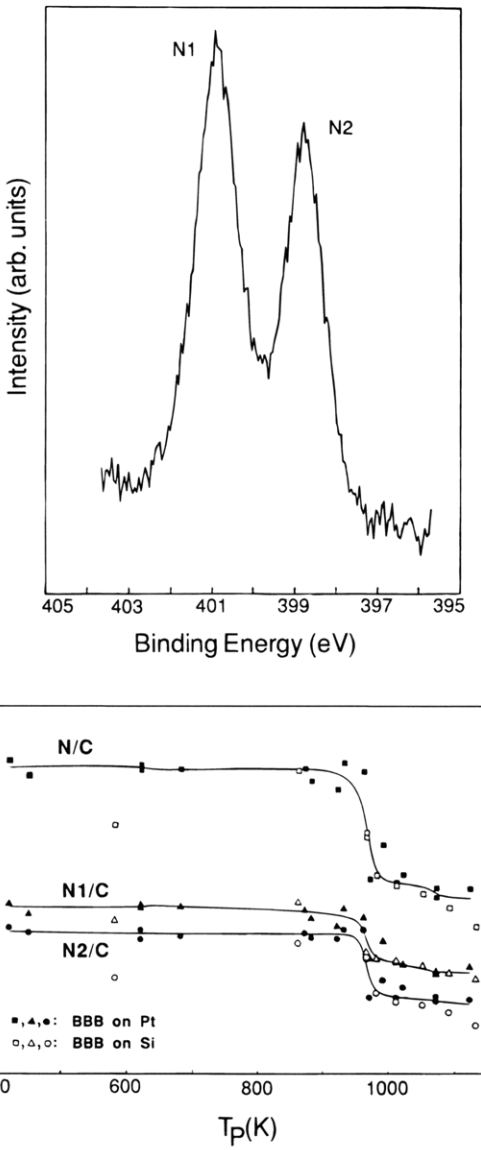

Figure 9. (A, top) XPS Mg Kα spectrum in the N1s range taken from a BBB film after annealing to 980 K. (B, bottom) The intensity ratios of the N1s and C1s core levels are plotted as a function of the annealing temperature. The ratios are determined from the intensities in the XPS spectra. N1 and N2 denotes the two components of the nitrogen emission as shown in Figure 10A.

annealing temperatures below 400 K. In a detailed analysis we find that the relative intensities of the two contributions amount to 0.86. This relative intensity ratio is stable and does not change with the annealing temperature.[10] Only in a very sharp temperature range around 950 K is there a small but remarkable change to 0.63 as shown in Figure 9B. This transition was observed for several samples investigated and found to be independent of the substrate used (Pt foils or Si wafers with natural oxides).[10] This distinct change is also observed for the relative intensities of the C1s and the N1s core levels (Figure 9B). The N/C ratio is 0.125 and varies at the transition temperature to values below 0.1. Consequently, the XPS intensity ratios reveal that two phases exist which can be identified by their different C1s and N1s relative intensities. In both phases the relative intensities are close to the ideal stoichiometric values of the films. For annealing temperatures below 950 K the emission at lower binding

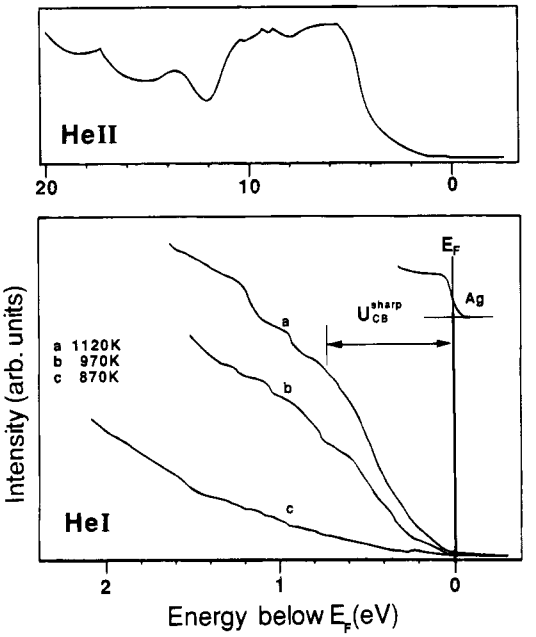

Figure 10. (A) Valence-band UPS (HeII) spectrum of a BBB film annealed to 1120 K. (B) Range next to the Fermi edge displayed for films annealed to different temperatures for the HeI spectra. For comparison the metallic Fermi edge of a clean Ag foil is also shown. The size of the pseudogap is indicated in the figure.

energy (398.7 eV) dominates. The emission at higher binding energy (400.8 eV) cannot be resolved for temperatures below 400 K. At annealing temperatures over 950 K its intensity decreases more strongly than that of the main emission at 398.5 eV. In a microscopic picture, the XPS spectra of the N1s emission give evidence that there are two different N species in the BBB films. In the UPS data the structural transition is most marked. Below the transition there is an n-type doping as indicated by the distance of the VBM relative to E_F (Figure 10). The DOS increases only negligibly up to 970 K, whereas above the transition there is a finite DOS in the gap up to the Fermi energy, indicative of a metallic state. In Figure 10 the valence band of a BBB film annealed to 1120 K is shown (A). There is a pronounced emission in the range about 6 eV which is typical of C2p bands and of aromatic π-systems. In addition, there is a weak band which extends towards the Fermi energy E_F. In the lower part we show the region close to E_F in more detail for a sample which has been annealed at different temperatures in the UHV system (B). It is clear that there is a negligible density of states above 1.5 eV unless the annealing temperature exceeds 970 K. At temperatures above 970 K, there is a pronounced emission appearing close to E_F, however, the DOS at E_F decreases toward zero in these spectra.

Model Calculations. The shape of the BBB molecule may be discussed controversially: there may be a N=COH group rather than a carbonyl group associated with an open heterocycle, which in turn causes a twisted molecular structure instead of a rigid planar configuration like that shown in Figure 11A (quinoid form). Both structural possibilities could be expected to result in rather different behavior upon annealing, as the COH group will allow a partial decomposition and hence more easily permit a cross-linking between neighboring polymeric chains.

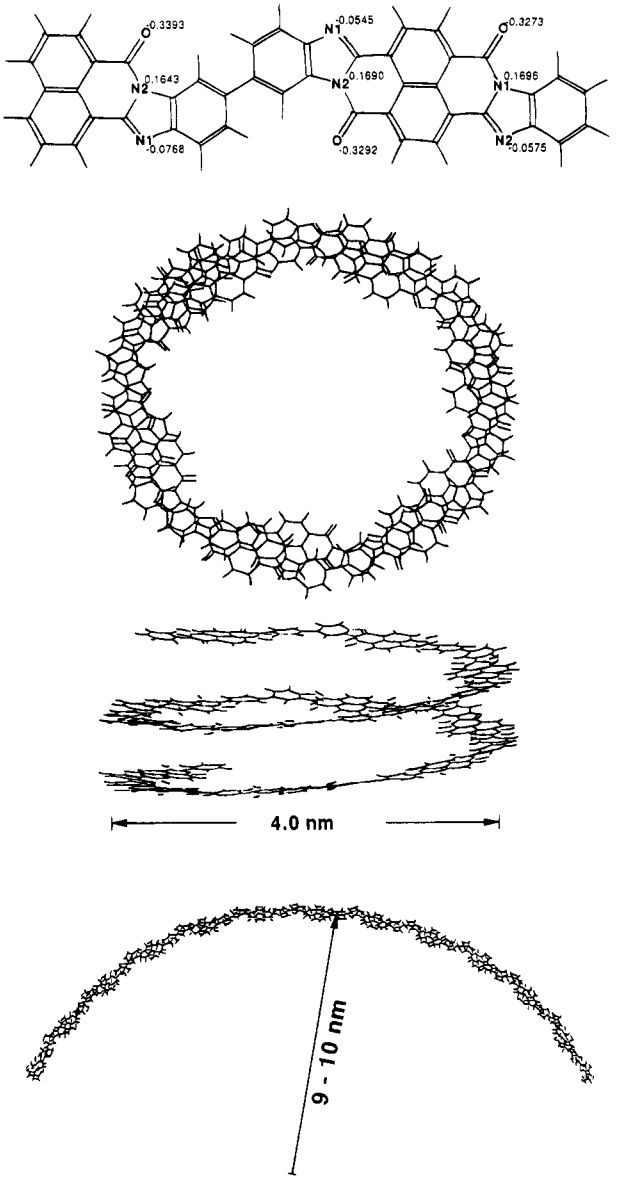

Figure 11. Monomeric model of the BBB polymer, derived from semiempirical MNDO calculations to optimize the geometric and electronic structure. The values of the partial charge at the nitrogen atoms are indicated (A, top). Helical arrangement of BBB as obtained after a force-field procedure. The diameter of the helical chain is about 4.0 nm (B, middle). Helical arrangements with diameters of up to 10 nm are possible by using an alternating cis–trans sequence, a sequence of which is shown in Figure 11C (bottom).

We have modeled a single BBB molecule to obtain the monomeric unit of the BBB polymer. Using the geometric optimization of a force-field routine, we in addition performed semiempirical MNDO[38] calculations to optimize both the structural as well as the electronic structure by minimizing the energy per bond. Our calculations thereby lead us to favor the planar quinoide configuration, although a simple straightforward semiempirical calculation does not account for the various electronic contributions of neighboring molecules. The obtained structure is shown in Figure 11A. It is highly planar, with the N=CO group incorporated within the plane of the overall π-system. The partial charges are

(38) MOPAC, Stewart, J. J. P. QCPE 455, Department of Chemistry, Indiana University, Bloomington, IN.

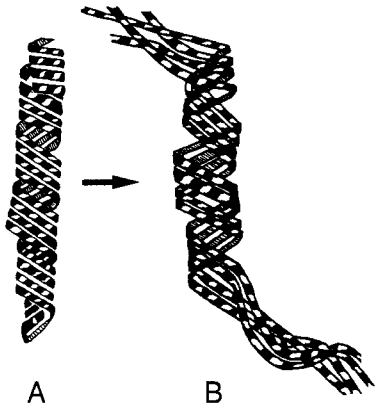

Figure 12. Model of a polymer strand consisting of four coiled fibers (A) and of its first unravelling step (B).

also determined from the MOPAC subroutines. They do indeed show that the two nitrogens are quite different. The charges on each amount to 0.16e−0.07e.

With this optimized monomeric structure, we have tried to find the most probable helical arrangement of a BBB polymer, using force-field routines. For a planar arrangement and an all-trans sequence, a linear polymer is obtained within the force-field optimization. Nevertheless, if we allow neighboring monomeric units to be twisted with respect to each other, we do obtain helical structures. We find the smallest helical diameter to occur for an arrangement in which the individual monomeric units are twisted by 6° as displayed in Figure 11B. Further arrangements with a larger diameter of the helix can be obtained by using an alternating cis−trans sequence of the N or C=O groups. The diameter of the helix depends on the details of conformational arrangement of subsequent monomeric units. It is smallest for the arrangement given in Figure 11B and becomes largest for an *N-trans,O-cis* arrangement. For the latter structure the diameter amounts to about 10 nm (see Figure 11C). In conclusion, a helical structure can be rationalized to originate from a nonplanarity within the monomeric structure. Also, starting from a planar monomere, helical structures can be built by a small inclination angle between neighboring molecules.

Discussion

Mesoscopic and Microscopic Structural Transitions and Dynamics. The STM measurements described above deal with the mesoscopic and microscopic structure of a bulk polymer film. Certainly, the scanned areas in the STM micrographs cover only a small range of the polymers surface. However, they provide new information on the dynamics of such polymeric films which are not available in spectroscopic studies. Spectroscopies, on the other hand, give integral information on the elemental composition and the chemical environment of the individual atoms, molecules, or functional side groups.

To explain and understand the great variety of phenotype structures of the material, we have to find the main principles of their construction and evolution. If these principles could be identified, we should have the possibility of distinguishing between precursor and intermediate structures which are representative of different steps within an evolutionary process. On the basis of only a few assumptions, we would like to demonstrate that all observed polymer structures can, in fact be understood as resulting from the dynamics within a single evolutionary process. Such structures should be regarded as precursor or intermediate structures to the final structure. The latter is achieved after passing the main structural transition at 950 K and results in polycrystalline graphitic carbon in an amorphous matrix.

For a better understanding of the evolutionary processes we have organized our results schematically in Figure 13. We first describe the structures as precursor structures obtained after annealing to 900 K. These are followed by several intermediate structures along the main routes of evolution (route A and B). We then focus on the patterns obtained at high lateral resolution. The intermediate structures are shown to be the starting point for a 2-dimensional polymerization. Finally, we discuss the structural transition which occurs upon annealing to 980 K and the features of the high-temperature phase. For the discussion of the STM data we have to assume that there are subtle differences in the temperature distribution on the samples during heat treatment. As a consequence we cannot rely on the temperature measurements alone but have to organize the patterns to find an evolutionary sequence; with the advantage that different patterns can be observed on a single sample.

To describe the individual steps of these transitions we introduce here some terms: If the monomers polymerize then a **polymeric chain** is created. A helical polymeric chain is named as a **fiber**, a coiled fiber as a **strand**, and a coiled strand as a **string**. The term **cord** is reserved to express the undefined nature of the polymeric element.

The Precursor Structure. As a precursor structure we consider the structural evolution that occurs within the BBB polymer upon annealing to 900 K. This precursor structure summarizes the critical parameters of the BBB polymers starting at the room-temperature polymerization process and the entropically enabled dynamics of these low-temperatures annealing steps. Due to the limited conductivities of such samples and their surface roughness these structures cannot be probed by STM. Consequently, the precursor structure we expect might be either a completely irregular arrangement of short polymeric strings of BBB or may consist of rather long polymeric cords with an average length of several hundreds of nanometers. This precursor structure should have cord widths large enough to allow for a large-scale orientation of the individual polymer strands which should amount to at least 30−40 nm. The size of such a large string is sufficient to allow a further reorganization by folding, cross-linking, segmentation, or decomposition.

There is some evidence for the existence of large precursor fibers in the observed patterns in the BBB films annealed below 900 K. We have not been able to record such a large precursor cord in complete. We suppose that the rough surface topology associated with it disables an access by STM. However, we do find a rudimentary structure which might be an indication for the existence of such a precursor structure. The corresponding STM pattern is displayed in Figure 2B. The

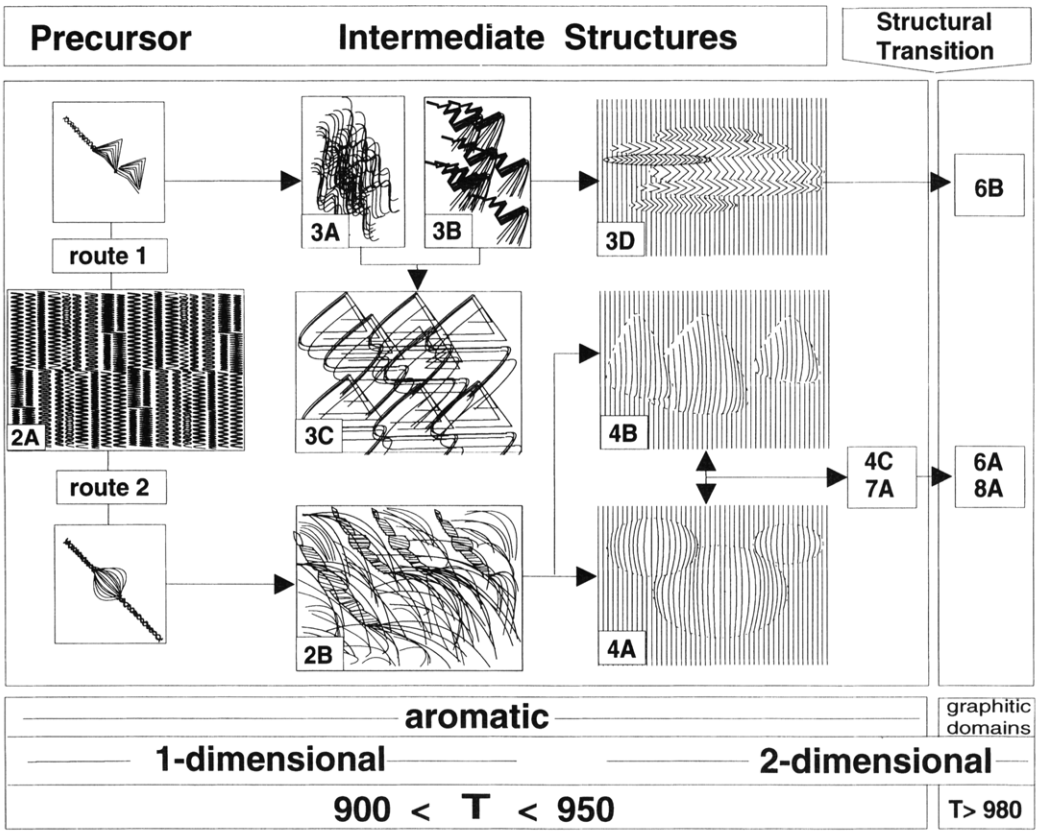

Figure 13. Schematical description of the structural evolution of the low-temperature phase of BBB films. With increasing temperature (900−950 K) the evolutionary process of the precursor structures (2A, 2B) can be understood as a general unravelling of polymer cords. On the precursor level the polymer is purely 1-dimensional aromatic. The polymer creates a matrix of multiple parallel ordered and coiled strings consisting of polymer chains, fibers, and strands. With increasing temperature within a single string, unravelling starts. Small differences in this process, caused by different flexibilities of the cords, are due to the creation of some intermediate structures (routes A and B). Unravelling on the string level leads to structures which were displayed in Figures 2B and 3A−C. The 1-dimensional ordering is reduced and cross-connecting between the strands and fibers occurs. During the course of this procedure an increase of interaction between fibers results from the creation of 2-dimensional patterns (Figures 3D, 4A, and 4B). After this unravelling and the creation of 2-dimensional fiber structures, the next step of the evolutionary process commences by a further increase of temperature (>950 K) and comprises the prime structure of BBB films. The purely aromatic precursor and intermediate structures (Figures 3D, 4C) are then displaced by the occurance of graphitic structures (Figure 6A,B) in the course of which the structural transition is indicated.

segmented and wound cord (string, A) on the left side of the image can be visualized as a rudiment of the expected precursor structure.

The fact that in these micrographs we observe exclusively strands of different widths suggests that BBB favors polymerizing in large strands. Indeed, our force-field calculations support this idea as helical structures can be rationalized to originate from BBB molecules which are slightly inclined to each other. For a helical arrangement the monomeric BBB must not be distorted itself. Amorphous ranges may also exist but are not probed by STM. Consequently, the helical precursors may be minority species.

In this context, there appears another structure which we believe to be an ultimate consequence of the rudimentary precursor structure. This precursor structure consists of the very regular arrangement of strands displayed in Figure 2A. The STM pattern shown in Figure 2A reveals some promising aspects for the criteria of a supposed precursor structure. These are the many fold wound strands consisting of a few fibers with an almost perfect parallel ordering which indicate a low interaction between the individual cords. A statistical cord-width evaluation is given in Figure 5A. It reveals a homogeneous distribution curve for the diameters of the observed helices between 4.0 and 11.0 nm with a maximum at 7.3 nm.

In general, there is a low number of defects with the appearance of cross connections. Nevertheless, we also find some defects within the otherwise regular pattern. For example, in the upper left hand part of the STM-image (Figure 2A) a plaiting of cords can be seen along the bars (A). Some cords show a segmentation (B) with furrows running diagonal to the direction of the cord indicating the helical nature of the strands. A cross-connection between cords is indicated by an arrow (C).

Two Routes along the Structural Transitions. Starting from the precursor structures (Figure 2) discussed above, we now wish to describe two routes for the evolution of the polymer cords. Both routes lead to a condensation of different intermediate structures and then finally to the structural transition which is observed around 950 K. The two routes (A, B) of evolution will be discussed separately.

The first route A is described in a sequence of images in Figure 3. This sequence starts with the precursor in Figure 2A and leads to the condensed intermediate structure in Figure 3D as illustrated schematically in Figure 13. If the cords of the precursor are ordered parallel to the surface plane (Figure 2A), an increase of

temperature may cause an unravelling, and the resulting expansion of the cords may then lead to a zigzag pattern of strands (Figure 3A). Further expansion results in an unravelling of the subunits and creates polymer ribbons consisting of parallel fibers with a smaller diameter. The ribbons may be folded and may reflect the rudimentary helical character of the precursor cords (Figure 3B). Helical structures will appear in the STM projection as parallel ordered strands and characteristic crossing overs, both of which are found in the described micrographs. If more and more strands unravel, a complex framework is observed which consists of triangular ordered fibers (Figure 3C). As a consequence of the unravelling, the polymer fibers are no longer planar but are lifted and can merge to build triagonal flakes at the surface which are aligned one behind the other like fallen dominos. The result of this process is a new condensed three-dimensional structure (Figure 3D).

The second route B of the evolution process starts again in Figure 2. The unravelling of the macroscopic precursor cords (20−30 nm) leads not to a parallel alignment to the surface plane but to a dipping in. This route is also observed and illustrated with the sequence of images beginning with Figure 2B and followed by Figure 4. The pattern shown in Figure 4C is the second of the two observed intermediate structures. This second route B is based on the same principles deduced from route A, but the unravelling of the strands does not start solely at their ends, creating ribbons of polymer fibers, because they are not aligned parallel to the surface and so they are less flexible. If the cords dip in in a parallel orientation a more or less undulating topology is created (Figure 4A,B).

If a cord consists only of a single multiple wound fiber, the unravelling process should become energetically favorable in contrast to cords consisting of more than one wound fiber. This is possibly expressed in the generation of some different structures during the evolution process. The intermediate structure (Figure 4C) can be understood as consisting of all these elemental unravelling steps.

The described transitions from precursor structures to aligned patches of polymer chains is a consequence of the polymer dynamics. With a high mobility of the polymeric strands, the annealing procedure enables unfolding and unravelling processes which are not favored energetically at lower temperatures. We also like to emphasize that the structural features are characteristic of bulk polymers and are certainly not caused by substrate or tip artifacts. The reader may ask why we argue that the evolutionary processes described in Figures 3 and 4 is to runs in the described and not in the opposite direction. Our statement is mainly based on two facts which can be deduced from the geometrical structures. First, the polymer strands and fibers described in the images Figures 2 and 3 were no longer observable after annealing to 980 K. These structures must arise from variations occurring after annealing to around 900 K. Second, there are equivalent structures in the main patterns observed after annealing to 980 K which indicate that the direction of the evolution process as here described is correct.

We now will compare the two final patterns of Figure 3D and Figure 4C which describe the evolution along routes A and B starting from the precursor structure. Both reflect the dynamics of the polymer strands and show that there are several similarities, although the overall patterns seem to be quite different. The different kind of fibers and the different ways of unravelling might be the main reasons for the creation of spherical or triagonally formed structural elements. A further indication is the average distance between the fibers within the structural elements (scales) of the two corresponding structures. In the first case (Figure 4A) the distance is about 3.7 nm and in the second 4.2 nm in agreement with the semi-empirical calculations (Figure 4B).

Description of the Structural Transition. With STM best resolution can be reached if the surface is flat, crystalline (or at least well ordered) and of smooth topology, and the material should have a good conductivity. In contrast to the high-temperature phase, the low-temperature phase fullfills none of these criteria. Nevertheless a resolution of the corrugation in the molecular rage could be achieved.

Below the structural transition molecular resolution is obtained although the obtained patterns do not exhibit a significantly long-range order. The high-resolution measurements on BBB samples annealed to 900 K reveal the existence of ordered polymer structures with an almost constant distance inbetween. Some of the imaged structure elements show a helical shape with a length of 1.5 nm or more. We find that these would polymer chains are the most prominent features in these patterns. Their irregular arrangement may be one of the main reasons for the weak resolution, as the atomic or molecular corrugation would appear better if the plane of unwound chains caused a flat topological surface. The wound shape of the chains is of great importance for the development of the structural transition. It reflects the potential of the BBB monomer and of the assembled polymer to create flexible cords. The latter are able to generate many kinds of phenotypes. Thereby, the structural variations become enabled and may be initiated at defect sites as shown in Figure 2A.

The annealing step at 980 K does not change the structural properties of the polymer films. As shown in Figure 6 the observed structures show an obvious relationship with the end structures obtained after the previous annealing step to 900 K (Figures 3D and 4C). The triagonal or spherical elements or scales in the structure of films annealed to 900 K are almost maintained after annealing to 980 K. The main difference is that the structural elements appear to be glued together. The manyfold structural transitions within the evolutionary process of BBB polymer films are based on the high flexibility of differently would polymer cords caused by low interaction. This is characteristic of the intermediate structures. During the evolutionary process or by increasing temperature a general unravelling of the polymer cords occurs. The changes in the cord-width distributions explained in Figure 5 reflect the evolution of the polymer structure. The process can be generally described by its two main properties: First, the standardization of the cord width leading to higher order and consequently to an increase of the cord-to-cord interaction. Second, the tendency to form uniform cord widths of around 4.0 nm during the evolutionary processes seems to be a major prerequisite for the

creation of more stable structural elements. This behavior again points to a two-dimensional polymerization. The structure of BBB films has now reached its highest grade of order on a molecular scale. Thereby the local order is increased and STM images with high resolution can be taken. The observed corrugation width is about 0.5 nm and is of the order of molecular dimensions.

Beyond the structural transition atomic resolution is obtained at several patches of BBB films annealed to 980 and 1120 K. Knowledge of the precursor and intermediate structures, as well as their structural changes toward a 2-dimensional polymerization below 980 K is a necessary prerequisite to understand the transition. Due to the increased local order, STM patterns could be obtained with atomic resolution. These micrographs reveal that it is the next step of evolution induced by annealing beyond 980 K which changes the corrugation in that the corrugation-width is reduced to 0.23 nm. This value is almost exactly the measurable corrugation width (by STM) of the atoms on graphite on the (0001) surface.[39]

We conclude that the reason for the structural transition is in the change of the molecular aromatic corrugation toward the graphitic corrugation and indicates the onset of carbonization. Our STM patterns obtained for BBB films annealed to 1120 K support this assumption as they again show well-corrugated crystalline ranges with the graphitic corrugation width. However, the size of the graphitic ranges is increased considerably. We like to mention that recent scanning force microscopy and scanning electron microscopy measurements of polypyrrole films (of about 10 μm thickness) revealed that this polymer also has two main structures. The first shows large polymer cords which are helical shaped, the second symmetrical spherically ordered features.[40]

We here summarize that after annealing to 900 K, BBB is purely an organic material and shows the properties of a polymer. These are reflected in the dynamics of the structure and the existence of cords and helixes, as well as the aromatic corrugation-widths. The transition at 950 K converts this structure to the high-temperature phase where the corrugation is no longer aromatic but graphitic. In this phase, BBB films resemble more an inorganic material with crystalline structures which are more typical of glassy carbon[9] or pyrolytic polymers.[15-19]

Electronic Structure. The electronic structure of the BBB films and the influence of the structural changes induced by annealing can be summarized by the XPS and UPS spectra given in Figures 9 and 10. In the XPS data the existence of the two peaks in the N1s region indicates that the polymer is stable for temperatures up to 1100 K. Both XPS and UPS data show that there is a structural transition which occurs after annealing to around 950 K. We observe a decrease of the N/C ratio and a significant broadening of the O1s, N1s, and C1s signals. The UPS data show a Fermi edge formed above 950 K, indicative of metallic behavior. We also deduce that BBB behaves as a n-type doped semiconductor at low temperatures, whereas p-type doping is usually observed in most organic polymers.[35]

Stoichiometric Intensities and Stability. The stability of the BBB monomer can be followed by the N/C ratio as determined by XPS relative intensities of the N1s and C1s core levels. For stoichiometric films the ratio is expected to be 1:9 (0.9); indeed, we found a value of 1:8 (0.125). For films annealed above the structural transition (950 K) the ratio decreases to 1:13 (0.075). Nevertheless, the existence and the relative intensities of the two N species indicate that the BBB unit is at least partially maintained even after annealing to 1000 K. It also indicates that main parts of the sample are covered with the amorphous polymeric material, whereas in some parts planar graphitic domains are formed. Only the latter are accessible for the STM tip. Thereby, we are not able to deduce from the N1s and O1s emission in the XPS spectra whether in these parts there are nitrogen- or oxygen-containing side groups incorporated. Certainly these side groups exist in the polymeric matrix. However, from the high conductivities we might expect that nitrogen or oxygen may act as dopants also in the graphitic domains.

Fine Structure of the N1s Emission. In the XPS data a splitting of the N1s signal of about 2 eV is observed for all temperatures, except in the unannealed samples on Ta foil and on Si wafers. It indicates a charge distribution which might be caused by the different chemical environments of the two nitrogen atoms. There are several reasonable explanations for the two nitrogens atoms to appear at different binding energies. First, there are different electronegativities which may be induced by the carbonyl group at the N1 atom. This effect is likely to be enhanced by the absence of any double bond at the N1 atom and the absence of mesomeric charge fluctuations. Second, a completely different explanation can be given when the aduction of OH groups to the N2 atom is considered. In this explanation the N1 atom contributes to the π-system of the BBB molecule, whereas the other one is localized at the NCO group. These two explanations consider different chemical environments and hence consider the ground-state properties of the nitrogen atoms probed by XPS.

A further physical origin which may be responsible for a split signal considers different screening mechanisms for the unequal C−N bonds in the final state. Different screening is expected to become the core hole excited in one of the two N atoms is stabilized in the large π-system. Indeed, there are differences along the polymerization route as the carbonyl group prevents the generation of a mesomeric quinoid structure via its neighboring N atom. The mesomeric quinoide structure forms a long π-system including the N2 atoms but not the N1 atoms. Thereby, a core hole at the N2 atom is more localized and is less effectively screened. A cross check with fluorinated samples showed only a single N1s line.[10] Although an assignment as to which of the nitrogen emissions has disappeared is not possible, this observation gives direct evidence that due to the missing second N1s level, the split is caused by a charge polarization resulting from mesomeric double bonds. A detailed analysis for the fluorinated samples is not possible as charging problems due to the low conductivity are inherent in the technique. Here we would like to discuss whether the mechanism for the split is in the ground or in the final state. The fact that the split is not observed on unannealed samples (except on Pt) may

(39) Binnig, G.; Rohrer, H. *IBM J. Res. Dev.* **1986**, *30(4)*, 355.
(40) Schmeisser, D.; et al., to be published.

favor the initial state arguments, as the addition reaction of a OH group has to be activated and hence the split should not exist for the room-temperature sample preparation procedure. On the other hand, the model calculation described in section 3.3 revealed a huge difference in the partial charges of 0.2e between the N1 and N2 atoms. As a consequence, the split must arise predominantly from the ground-state properties of the BBB monomer and not from relaxation phenomena which hence are of minor significance.

We therefore believe that in the spectra taken prior to the annealing procedures adsorbed or incorporated water is preferentially interacting via the carbonyl groups and makes the two nitrogen atoms similar to each other. Annealing removes the adsorbed water and causes the differences in the partial charges to split the N1s XPS signal, which is in agreement with the MNDO results.

It should be mentioned that an uncoiling of helical BBB strands also may release the NCO groups which are responsible for the intrachain cross-linking via H bonds. Thereby the changes in the relative intensities around 970 K may be rationalized.

Valence Band Spectra. The valence band spectra provide a further indication of the high thermal stability of the BBB films. It was found that the HeII valence band spectra do not change significantly upon annealing. There is only a general broadening of all structures, but the main features which are indicative of BBB monomers are still observable.

In the metallic state of 2-dimensional cross-linked polypyrrole and polyfuran films, an unstructured emission pattern with very low intensity has been observed and is interpreted in terms of a graphitic electronic structure.[8] On the other hand, C2p-derived states with significant intensities are observed in 1-dimensional polypyrrole films and interpreted in terms of polaronic states.[37] The valence band spectra of BBB films annealed above 970 K are not indicative of unstructured graphite but their emission pattern in the range close to the Fermi energy indicates that there must be C2p-derived states responsible for the considerable intensity. According to this comparison with polypyrrole films, we would like to argue that the electronic structure close to the phase transition is determined by polaronic states.

The appearance of a pseudogap in these BBB films is in accordance with polaronic states and a high carrier density. Actually, the EPR results[11,12] indicate that around the structural transition at about 950 K the spin density has a maximum and decreases rapidly for higher annealing temperatures. The transition to a graphitic state at elevated temperatures (T > 1120 K) is also shown in the valence band spectra by the strongly reduced intensity near the Fermi energy.

The absence of a metallic Fermi edge is associated with the appearance of a pseudogap in the density of states at the Fermi level. Again this finding is similar to the UPS results obtained for highly doped polypyrrole films and is interpreted in terms of the appearance of long-range Coulomb interaction between the polarons. From the size of the pseudogap the ratio of U/W can be determined directly.

Conductivities. The conductivity of BBB films indicates two different regions with regard to the changes upon the annealing procedures.[11] There is a strong increase in the conductivity of the materials annealed close to the transition, whereas for films annealed to higher temperatures, the conductivity is high (50 S cm^{-1}) but no longer changes significantly upon annealing.

In the range below the structural transition the increase of the conductivity may be assigned to a cross polymerization via additional OH groups which are still present in the films because of the polymerization process in water. Such a cross connection is enabled by the different partial charges at the two unequal nitrogen atoms which may be even enhanced by OH groups. A cross polymerization would induce a charge separation in the BBB monomers. This process may be visualized as a doping by polarons in the already existing 1-dimensional ladder-type polymer. Such mechanisms are well-known to occur in conjugated polymers, e.g., polypyrrole and polyacetylene are known to enhance the conductivity by several orders of magnitude.[35]

However, there are some differences, such as in BBB an OH group induces an extra electron corresponding to n-type doping. An n-type doping is actually reported for low doping levels,[11] whereas at high doping levels the doping is p-type doping. Otherwise, not only OH groups but any structural defect may be stabilized by electron–phonon interactions in a polymeric material. Most of such defects cause a p-type polaron, and we are here led to assume a high degree of structural defects within the films by our STM micrographs. If we assume structural defects to be stabilized as polarons, then these will cause the conductivity increase in the p-type doping region. Furthermore, heavy polaron doping causes a broadening of the polaron bands which finally leads to a metallic DOS. Such a description is in accordance with the findings for polypyrrole.[35]

The different charge distribution of the C–N bonds allows the formation of a 2-dimensional network with the observed metallic density of states. In this state, an estimate of the actual carrier densities from the width of the pseudogap can be derived. It should be noted that the doping by polarons is not associated with the structural transition but that the transition to a 2-dimensional graphitic structure is responsible for a 2-dimensional conductivity which no longer causes an significant increase upon annealing to higher temperatures. In the electronic structure probed by the UPS valence band spectra a graphitic DOS has a very low intensity and an unstructured emission pattern. We are therefore not able to distinguish between the appearance of a pseudogap and the appearance of the 2-dimensional graphitic phase. In films annealed to temperatures above 1120 K, the conductivity is determined by the size and distribution of 2-dimensional domains with a graphitic structure.

Summary

We have studied changes in the electronic and real-space structures of BBB films after annealing between 900 and 1100 K. A direct comparison of the different techniques provides complementary informations, although the films are polycrystalline at all temperature treatments. In addition, the electronic structure and

the presence of helical arrangements are confirmed by semiempirical model calculations.

Only at temperatures above 1000 K is the formation of graphitic domains evident in STM patterns as well as in the electronic structure. For films annealed to lower temperatures, the STM provides a microscopic view and has a sufficient molecular resolution for discerning smooth ranges, whereas photoelectron spectroscopy can also probe the surrounding amorphous ranges. The STM micrographs allow us to conclude that an irreversible structural transition occurs when the films are annealed at temperatures up to 980 K.

In the electronic structure that transition is shown in the relative XPS intensities, while in the valence band data there is a change from a semiconductive to a metallic-like DOS. The structural transition is associated with the formation of 2-dimensional graphitic domains with a characteristically low DOS near E_F. The structural transition at 950 K also shows up in the conductivities and EPR data.[11,12] At low temperatures polaronic defects cause an increase in the conductivity which remains almost stable above the transition temperature. The spin density initially increases due to the existence of polaronic states but then decreases above the transition due to the increasing number of 2-dimensional graphitic domains.

The transition is shown in the STM data as a change from a molecular corrugation to an atomic corrugation which can be determined by the graphitic C−C distances.

There are several precursor structures which are formed upon annealing to temperatures below 950 K and which reflect the high dynamics involved in annealed polymeric films. The precursor structures initially from a large helical strand, which with increasing temperature shows an increasing number of defects. At such defects, the formation of fish scales commences either at unwound or cross-linked helical subunits; these have an average diameter of around 70 nm and a 2-dimensional arrangement of neighbored BBB fibers.

Acknowledgment. We wish to thank D. Davidov, I. Belaish, S. Roth, and P. Bätz for stimulating discussions and W. Neu for experimental assistance.